ACS OMEGA

Open Access

This article is licensed under CC-BY-NC-ND 4.0

http://pubs.acs.org/journal/acsodf

Article

Photonic Cooler Based on Multistacked Thin Films with Near-Infrared Filter Properties

Brahim Aïssa* and Mohammad Istiaque Hossain

Cite This: *ACS Omega* 2024, 9, 3295−3304

Read Online

ACCESS | Metrics & More | Article Recommendations

ABSTRACT: We report on the development of a multistacked configuration of a photonic cooler for implementation in sunny and arid regions. The optimized multistacking structure considers TiO_x as a top layer, NiO_x as the buffer layer, and Ag as a hot mirror (i.e., a reflective layer of the NIR light spectrum). The entire stacked layers were deposited in situ without breaking the vacuum. The oxide layers were grown reactively under an oxygen medium at a deposition pressure of 2×10^{-4} Torr. The level of TiO_x surface wettability was demonstrated to be controlled by the oxygen flow during the film growth process, which may additionally provide a self-cleaning property to the IR filters. By combining low refractive index layers (i.e., TiO_x) with the high refractive index of the metal oxides (i.e., NiO_x) along with the metal layers (i.e., Ag, Al), the photonic filtration (i.e., cutoff) of the infrared spectrum was successfully achieved while keeping the light transmittance of the visible (vis) light above 50%. Different structures with different thicknesses have been systematically assessed, including TiO_x/NiO*x*/Ag, TiO_x/NiO_x/Al, TiO_x/MoO_x/Ag, and TiO_x/MoO_x/Al. Furthermore, numerical simulations were carried out using SCAPS-1D and OptiLayer software to evaluate the application of these filters on silicon solar cells, considering the experimental electrical and optical parameters for each explicit layer of the device. Our results confirm that the development of such coatings with a scalable thin film growth process may have a real commercialization potential due to their multifunctionalities such as IR filtering, antireflection coating in the vis range, and antisoiling properties.

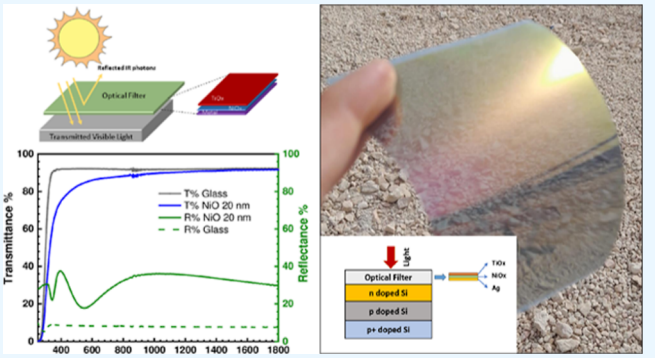

1. INTRODUCTION

The radiated solar spectrum on earth has three main subbodies, namely, ultraviolet (UV), visible (vis), and infrared (IR). The proportion of the IR spectrum is higher than that of the vis and UV parts, with about 54% of incident radiation.[1] This part of the solar spectrum is the main reason behind heat generation, where the glass covering a photovoltaic (PV) panel, for instance, converts the accumulated IR wavelength into thermal heat.[2] In the context of PV, the panels' efficiency decreases as their temperature increases. Similarly, the energy consumption of a building increases significantly (i.e., for cooling purposes) due to this IR absorption phenomenon in the windows.[3]

Within the Gulf Cooperation Council (GCC) countries, the prevailing arid and sun-drenched conditions define a specific environmental context characterized by abundant sunlight and minimal humidity levels. These environmental attributes can significantly deviate from more typical settings, such as temperate or tropical climates, resulting in distinct requirements for the organisms and ecosystems inhabiting these areas. The sun-soaked and arid conditions create a unique and demanding ecological niche marked by limited water resources, extreme temperature fluctuations, and specialized adaptations. Organisms residing in these environments must develop specific strategies to flourish and withstand the formidable challenges they face. This underscores the vital significance of conservation initiatives aimed at preserving the fragile ecosystems present in arid regions.

IR filters, customarily engineered for heat mitigation, typically operate by selectively impeding a portion of the IR radiation emanating from the sun. These filters are crafted by using materials with specific optical properties, meticulously selected to impede or weaken particular wavelengths of IR light while allowing visible light to pass with minimal hindrance. The filter material is intentionally designed to preferentially absorb or obstruct the longer wavelengths of IR radiation, often found in the near-IR (NIR) or mid-IR spectrum, which is responsible for generating heat. Through this substantial

Received: August 2, 2023
Revised: December 21, 2023
Accepted: December 27, 2023
Published: January 11, 2024

© 2024 The Authors. Published by American Chemical Society

Table 1. Comparison of Different Photonic Coolers

specification	our development	ConverLight65[64]	ConverLight75[64]	oxide-based multilayer structure[65]	nitride-based multilayer structure[65]
fabrication technique	physical vapor deposition	physical vapor deposition	physical vapor deposition	physical vapor deposition	physical vapor deposition
cost	inexpensive due to the simple structure, no process temperature, and available materials	expensive due to the complex structure	expensive due to the complex structure	expensive due to the complex structure	expensive due to the complex structure
applications	broad (building windows to PV)	broad (building windows to PV)	broad (building windows to PV)	PV	PV
functionalities	NIR filter, daylight harvesting, and antisoiling coating	NIR filter	NIR filter	NIR filter	NIR filter
number of stacked layers	3	5	5	8	4

Table 2. Performance Indicators of Various Photonic Coolers

	our development	ConverLight65[64]	ConverLight75[64]
light transmittance	~78% in the vis range	~65% in the vis range	~75% in the vis range
light reflection	~75% in the IR range	~90% in the IR range	~80% in the IR range
ccalable	yes	yes	yes
stability	tested for 6 months, and samples did not change in terms of stoichiometry and morphology	NAE-4	NA
light weight	yes (as developed on flexible substrates)	NA	NA

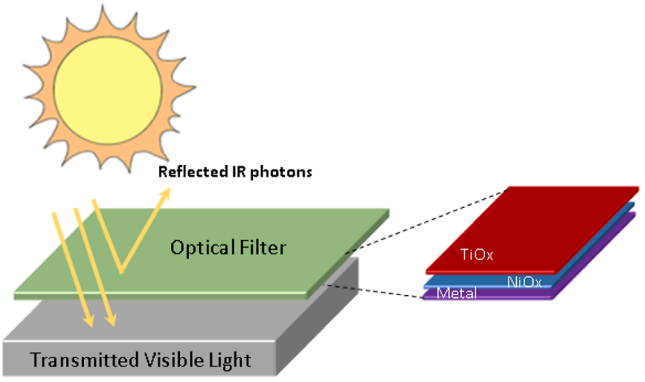

Figure 1. Schematic structure of an IR photonic filter.

interception of IR radiation, these filters effectively block a significant amount of heat. This reduction in heat transmission can be especially beneficial in environments characterized by abundant sunlight and a pronounced presence of IR energy such as sunny and arid conditions. It is important to recognize that the effectiveness of IR filters in reducing heat is contingent on various factors, including the specific filter design, the choice of materials, and the intensity of the IR radiation in the surrounding environment. Additionally, the extent of heat reduction may fluctuate depending on the circumstances and the type of filter employed. In summary, IR filters function under sunny and arid conditions by selectively obstructing IR radiation, thereby aiding in the mitigation of heat-related effects and contributing to a cooler atmosphere.

One promising solution for cooling PV panels is a photonic cooler based on the IR filtering of light. A photonic cooler is a device (or coating) used to control the heating of an object without the need for any moving parts or refrigerants. It works by reflecting IR radiation while allowing visible light to pass through, thus selectively cooling the object. The efficiency of a photonic cooler is dependent on the configuration of the IR filter. Ultimately, developing a coating to meet the purpose of reflecting the IR spectrum without altering the normal functionalities of the device is the ideal aim.[4]

An IR filter works by exploiting the fact that IR radiation has a wavelength longer than that of visible light. An IR filter can

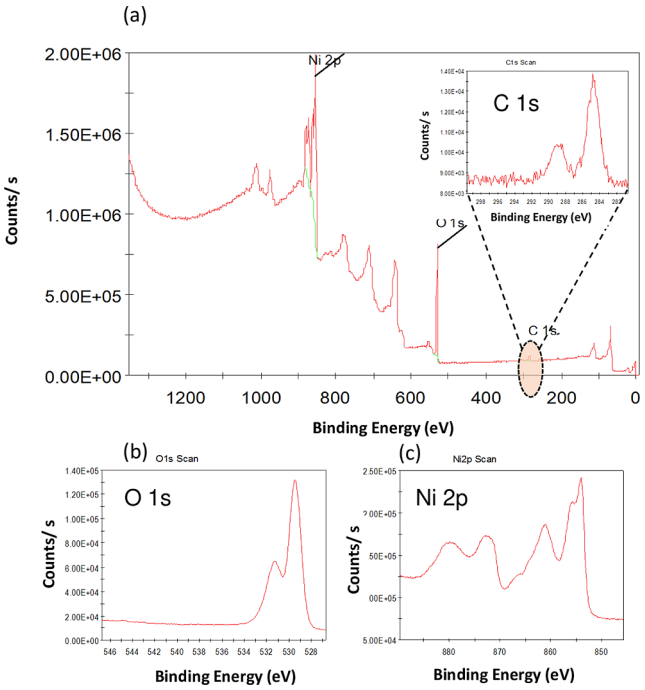

Figure 2. XPS survey of NiO layers grown at 2×10^{-4} Torr with 100 nm thickness. High-resolution XPS for (b) O 1s and (c) Ni 2p.

be made by depositing layers of thin films with different refractive indices on a specific substrate. The thickness and refractive index of each layer have to be carefully selected to create a filter that reflects or transmits IR radiation while allowing visible light to pass through it. A photonic cooler based on an IR filter has several advantages over other cooling methods. First, it is maintenance-free and has a long lifespan.[4] Second, it is a passive device, not consuming any energy. This makes it an ideal solution for cooling PV panels in a plant. Third, it is a lightweight and compact device, which makes it easy to install and integrate into existing PV systems.

A photonic cooler based on an IR filter can considerably improve the efficiency of PV panels. This improvement in efficiency can translate into significant cost savings over the

https://doi.org/10.1021/acsomega.3c05561
ACS Omega 2024, 9, 3295−3304

lifetime of a PV system. In addition to improving the efficiency of PV panels, a photonic cooler based on an IR filter can also increase their lifespan as they are affected by the operating temperature. In addition, by keeping the temperature of a PV panel lower, a photonic cooler can reduce the stress on the panel's components and extend its longevity.[5]

Up to now, multiple thin films of metallic layers such as Ag, Al, and Au have been suggested to be used as filters of the IR spectrum due to their capability of absorbing resonance frequencies in the IR range.[5] However, the stability of these metallic coatings is a major drawback.[6] Sandwich structures have then been developed, keeping such a metallic layer in between oxide layers.[7−10,25−30] The MoO_x/Ag/MoO_x structure was first proposed, yet oxygen diffusion of moly oxide became obvious, and in situ stress has resulted in fractured films,[8] resulting in poor light management in the vis region as scattering takes place in the top layer.[9] Consequently, developing an IR filter has to also meet the query of vis light maximization. Initial research works have dealt with doped transparent conductive oxide as they are thermally and chemically stable;[10−13] however, their large-scale deployment was not successful due to the low IR cutoff percentage.[14−19] NiO/Ag, NiO/Au, NiO/Ni, and NiO/Pt stacked layers were then developed for UV light filtration and photocatalytic activity, but the functionality of IR filtration was not met and remained a persistent technological challenge.[20−24] We conducted both experimental and numerical validations to confirm the feasibility of creating a photonic cooling system for smart windows. This technology utilizes nanofilms made from cost-effective oxide materials integrated with metal layers. Additionally, we have improved the IR filtration by adopting a stacking approach involving an inorganic metal oxide (with a low refractive index), followed by a metal oxide (with a high refractive index), and finally, a metal layer. This stacking arrangement enhances the stability of the photonic layers, thereby leading to a reduction in production costs. Our method for creating these stacked layers for large-scale applications involves the use of an e-beam evaporator without breaking the vacuum. We have successfully employed stacked layers composed of Ag/NiO_x/TiO_x, Al/NiO_x/TiO_x, Ag/MoO*x*/TiO*x*, and Al/MoO*x*/TiO*x* as IR filters to develop a cost-effective photonic cooling system. In our experimental investigations, we observed that NiO*x*/TiO*x* layers exhibited higher transmittance (T %) in the vis spectrum when compared with that of a single TiO*x* layer. However, as we moved into the NIR region, T % began to decline for both stacked layers. Subsequently, the introduction of a metal layer (either Ag or Al) has led to a wavelength cutoff starting at about 1100 nm by reflecting light.

In summary, our research has demonstrated the practicality of developing a low-cost photonic cooling system for smart windows using nanofilms made from cost-effective oxide materials integrated with metal layers. This technology offers improved IR filtration, enhanced stability through layer stacking, and cost savings in large-scale production processes.

So far, four metal oxide layers have demonstrated the required technical compatibility to develop such IR filters, namely, TiO_x,[25] SnO_x,[26] MoO_x,[27] and NiO_x.[28] The TiO_x layer has a large refractive index with an intrinsic self-cleaning property, making it a suitable candidate as a top layer for an IR filter, especially for dusty environments.[29] For both MoO_x and NiO_x, their optical properties are also appropriate to be integrated between a high refractive index layer and a metal layer.[5,30,32] Up to now, physical vapor deposition techniques have been proven to be the most relevant to grow such oxides, including RF/DC sputtering,[33−35] e-beam/thermal evaporation,[36−38] and atomic layer deposition.[39−41] Among these techniques, the e-beam shows good flexibility and a high capability in fabricating uniform layers.[42,43]

Usually, photonic coolers lack moving components, simplifying the manufacturing process and decreasing production expenses.[31] Our advanced cooler, for instance, comprises merely three layers, in contrast to traditional cooling systems. Nevertheless, the straightforward nature of photonic cooling technology facilitates seamless scalability for large-scale production, leading to additional reductions in manufacturing expenses. As shown in Table 1, other reference photonic coolers have more than 3 layers, which eventually leads to extra production costs.

Commercially available NIR filters have complex designs, are costly, and have limited applications and functionalities. A product named ConverLight65 has a light transmittance of 65% in its brightest stage and blocks 90% of the heat transfer in its darkest stage, whereas ConverLight75 has a light transmittance of 75% in its brightest stage and blocks 80% of the heat transfer in its darkest stage.[64] Hence, the development of a product with high performance. Table 2 compares various parameters of the developed photonic cooler with those of the conventional ones. As calculated, our developed optical filters confirm the significant temperature reduction (TR).

In general, absorptance (A) + transmittance (T) + reflectance (R) = 100%. For $R \approx 100\%$, $A \approx T \approx 0\%$, when the entire solar spectrum is reflected. In the proposed filter with the insertion of an optimized metal layer based on review, for wavelength λ (nm) = 780−2000, average $R \approx 75\%$. Considering all NIR photon absorption in NIR, $A + T \approx 25\%$. In summary, from the relevant literature, 100% absorption of IR wavelengths ≈70 °C temperature, considering $R \approx 75\% \approx$ 52.5 °C temperature, which confirms TR by ≈ 75%. Hence, the filter appears to be very promising for reducing temperature.

Optimizing the thickness of IR filters plays a vital role in tailoring their performance characteristics and optimizing their efficiency in handling IR light. IR light encompasses a wide range of wavelengths that extend beyond the human eye's perceptible range. Various applications demand the selective filtering of specific wavelengths or bands within this extensive IR spectrum. Modulating the filter's thickness serves as a method for precisely targeting and isolating particular IR wavelengths. This adjustment becomes imperative when the objective is either transmitting or obstructing particular wavelengths. For instance, in interference filters, where multiple layers of thin films are employed, meticulous control over the thickness of each layer is essential. This precise control enables the filter to discriminate and effectively manipulate the transmission or reflection of specific IR wavelengths. The optimization of thickness becomes a critical factor in achieving the desired interference pattern and, consequently, the desired filter performance. Furthermore, thickness optimization holds the potential to mitigate undesired optical effects such as reflections and stray light. Filters that are thoughtfully designed and optimized have the capacity to minimize these adverse effects, thereby significantly enhancing the overall performance of optical systems. Essentially, the process of thickness optimization for IR filters emerges as a pivotal strategy for customizing their optical

https://doi.org/10.1021/acsomega.3c05561
ACS Omega 2024, 9, 3295−3304

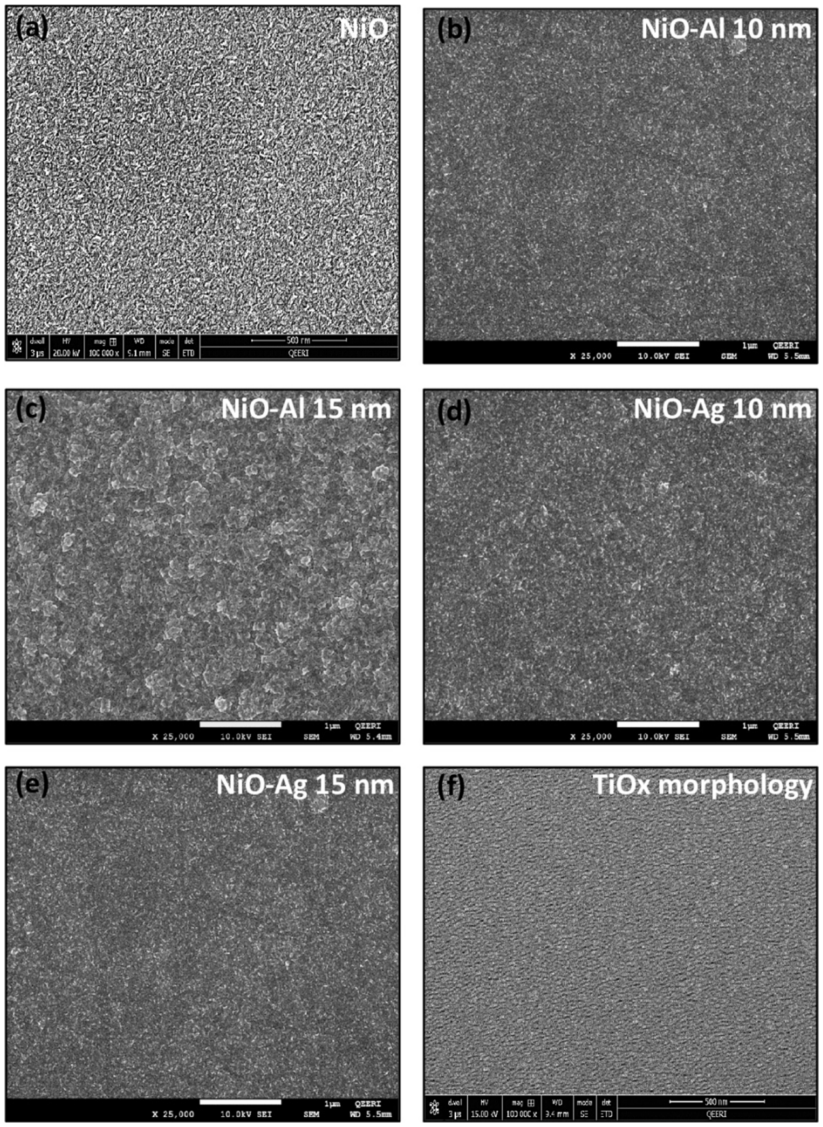

Figure 3. Top-view SEM images of NiO/metal layers: (a) NiO (300 nm), (b) NiO (100 nm)/Al (10 nm), (c) NiO (300 nm)/Al (20 m), (d) NiO (100 nm)/Ag (10 nm), (e) NiO (300 nm)/Ag (20 nm), and (f) TiO_x (50 nm) on NiO (300 nm).

characteristics to cater to specific applications. This optimization not only maximizes their operational efficiency but also ensures their capability to proficiently filter or transmit the intended IR wavelengths while concurrently minimizing any undesirable optical effects.

In this work, we report on the development of an efficient version of a metal-oxide/metal-oxide/metal multistack IR filter with multiple functionalities through an e-beam evaporation process that allows a high degree of control over the growth parameters without breaking the vacuum. Numerical simulations based on experimental parameters have been considered to meet the requirements of high T % in the vis range and high R % in the IR region. Results were applied to silicon solar cells to highlight the improvement in PV performance after IR filtration. Figure 1 illustrates the structure of these IR photonic cooler filters.

Relying on the inherent characteristics of conventional films, traditional radiative cooling films may face various challenges in hot and sunny regions. These proposed specialized films hold the promise of delivering a flexible coating that can adapt complex geometries, with an effective cooling solution in an environment with elevated temperatures; a circumstance where conventional radiative cooling technologies might struggle to maintain optimal performance. Additionally, the purpose of traditional IR filters, which involves blocking or manipulating specific wavelengths of IR radiation, may unintentionally contribute to increased heat retention within buildings. In settings where external temperatures are already high, the deployment of conventional IR filters could potentially intensify indoor heat levels, compromising the efficiency of cooling systems and the overall energy efficiency due to thermal stress. Furthermore, these properties may not effectively address dust-related issues when they are applied to PV panels.

2. METHODOLOGY

2.1. Material Preparation. NiO and TiO_x metal-oxide layers were reactively evaporated at room temperature (RT) with a growth rate of 1 Å/s and a deposition pressure of 2×10^{-4} Torr, under a constant oxygen flow of 20 sccm, using a Denton e-beam evaporation system. Later, the Al and Ag metal layers were evaporated at the same growth rate without any

https://doi.org/10.1021/acsomega.3c05561
ACS Omega 2024, 9, 3295−3304

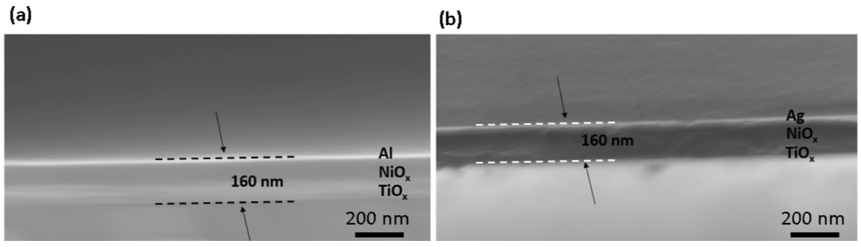

Figure 4. SEM images of NIR-stacked films: (a) TiO_x stacked over NiO_x/Al and (b) TiO_x stacked over NiO_x/Ag.

oxygen supply. Samples were optically measured using UV−vis (UV−vis/PerkinElmer Lambda) spectroscopy. The wetting behavior of the film's surfaces was characterized using Kruss contact angle measurements. A Dektak 3D stylus was used to characterize surface topology, whereas JEOL 7610 field-emission scanning electron microscopy was engaged to study the microstructure and the morphology of the layers. Structural characterization was carried out using X-ray photoelectron spectroscopy (XPS), performed at 100 eV with 1 scan and 20 eV for specific and narrow bandwidth with 10 scans (i.e., for high-resolution XPS), using a monochromatic Al Kα from Thermo Fisher Scientific. Spectral analysis and peak fitting were carried out using "Avantage" software. At the beginning of the process, a thickness optimization study was systematically performed for each layer to maximize its optical properties. To understand the thickness influence, we have varied the thickness for both NiO and TiO_x between 50 and 250 nm, whereas the metal layer was varied from 5 to 20 nm in an iterative manner. The employed tool allows us to deposit multilayers in a stacked manner without breaking the vacuum. The glass substrates with a dimension of 1″ × 1″ were sonicated and cleaned using different solvents such as DI water, acetone, and isopropanol. Later, substrates were dried under inert nitrogen. All source materials were purchased from Kurt J. Lesker with 99.9995% purity.

2.2. Numerical Simulation. To simulate the effect of the developed coatings on solar cell performance and the thermal budget these filters may compensate for, numerical simulations were carried out using SCAPS-1D and OptiLayer software.[54−56] A silicon solar cell structure has been selected for this study. This analyzer utilizes both electrical and optical parameters for each explicit layer of the device. In general, the simulator derives a finite approach to solve carriers' drift as well as diffusion equations to understand the mobility within the device. In addition, it allows introducing defects as concentrations or states to mimic a real device structure. This analyzer also adapts Poisson's equation, which is used to model the space charge-dependent gradient across the device, and continuity equations are then used to calculate the charge transport.

3. RESULTS AND DISCUSSION

3.1. Structural Properties. Figure 2 shows the XPS analysis of the deposited NiO thin films deposited at 2 × 10^{-4} Torr with different thicknesses, namely, 50, 100, 200, and 300 nm. All of the peaks were fitted by Avantage software. As studied, the survey spectrum confirms the growth of pristine nickel oxide with a stoichiometry approaching that of NiO, showing minimal carbon contamination.

To consider a precise amount of oxygen, the amount of oxygen attached to carbon atoms was deducted from the total number of oxygen atoms. In general, the deposition pressure

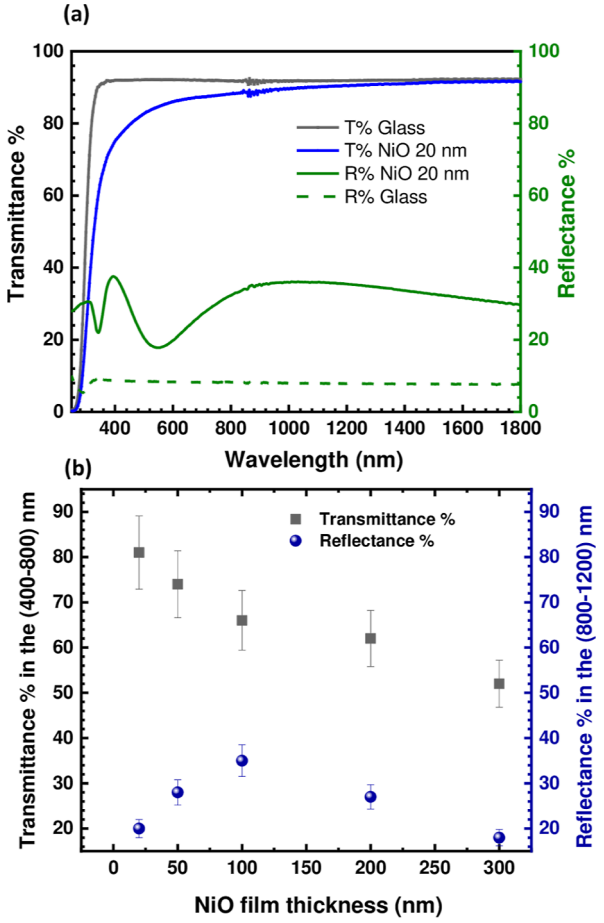

Figure 5. UV−vis results of NiO_x layers grown at 2 × 10^{-4} Torr with different thicknesses: (a) typical example of T % and R % of NiO_x of 20 nm thickness and (b) summary of T % and R % of NiO_x films with different thicknesses.

plays a significant role in making the surface oxygen-rich. A slight stoichiometric deviation range was found, which confirmed the optimized growth of such metal oxide layers. The measured oxygen spectra were mainly carbon-related and oxide-related. In NiO_x samples, the stoichiometry was around $NiO_{0.84}$.[44−46]

3.2. Morphological Analysis. Figure 3a shows typical top-view SEM images of the evaporated NiO_x with a 300 nm thickness. Figure 3b−e displays the top-view images of NiO_x films after stacking with metal layers (Al and/or Ag) with two thicknesses of 10 and 15 nm, respectively. As demonstrated by these images, all deposited stacked layers consist of closely packed nanocrystals that are dense, homogeneous, and without any pinholes or cracks, covering uniformly the entire sample surface. These features are essential to develop high-end

https://doi.org/10.1021/acsomega.3c05561
ACS Omega 2024, 9, 3295−3304

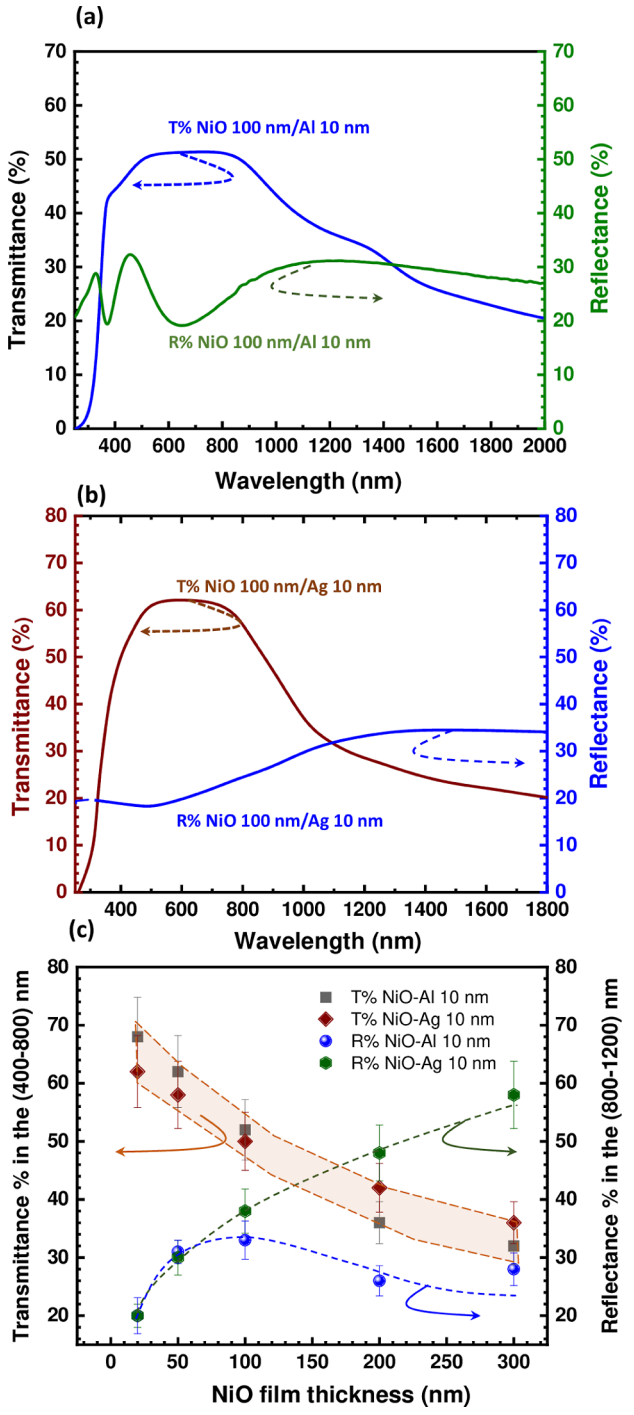

Figure 6. UV−vis results of NiO/metal layers grown with different thicknesses. (a) Transmittance (%) and reflectance (%) of 100 nm thick NiO deposited on (a) 10 nm of Al and (b) 10 nm of Ag layers. (c) Variation of both *T* % and *R* % with respect to the NiO film thicknesses for two metals, namely, Al and Ag.

optical devices such as IR filters. Figure 3f shows evaporated TiO_x on top of NiO.

TiO_x/NiO_x/metal layers are characterized by a cross-sectional view, as shown in Figure 4. The thin films confirm pristine morphological features when observed in cross section. As found, the stacked films are uniform, homogeneous, and dense throughout the entire thickness. The total thickness of the stacked layers is approximately 160 nm, which matches the targeted thickness deposition.

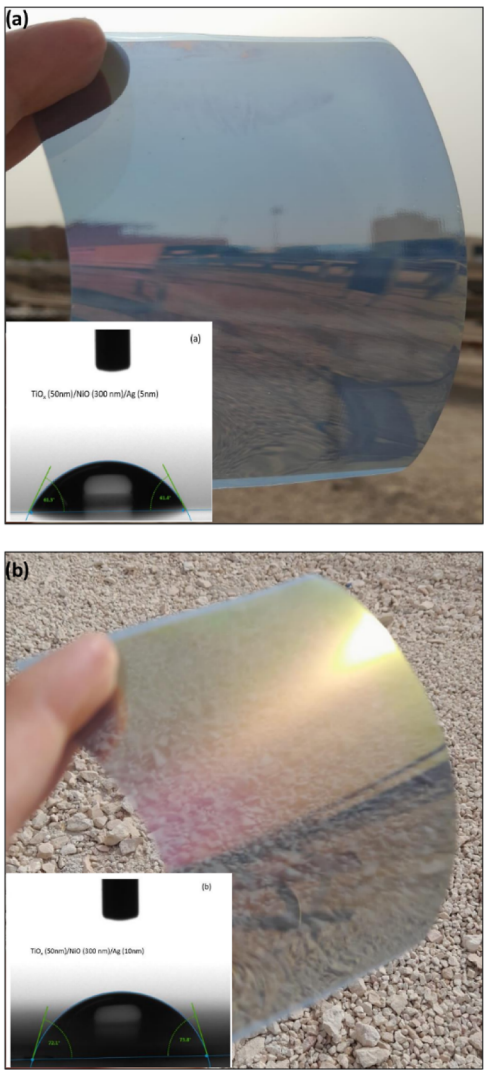

Figure 7. Optical photos of (a) TiO_x (50 nm)/NiO (100 nm)/Ag (10 nm) and (b) TiO_x (50 nm)/NiO (100 nm)/Ag (15 nm) filters. Insets show examples of the contact angle measurements performed on these flexible coatings.

3.3. Optical Properties. UV−vis spectroscopy was used to examine the optical properties of the stacked metal/metal oxide layers, where absorptance spectra were calculated using the following formula

$$A\ (\%) = 100 - (T + R) \quad (1)$$

where *A*, *T*, and *R* stand for absorptance, transmittance, and reflectance, respectively.

As measured and shown in Figure 5a, transmission and reflectance spectra vary with respect to wavelengths ranging from 200 to 2000 nm. Figure 5b summarizes the average *T* % measured in the visible (400−750 nm) range and the average *R* % measured in the IR (750−1200 nm) range as a function of the NiO_x thicknesses. While the transmittance is the highest (80%) for the 20 nm thick film and decreases expectedly with respect to the film thickness, the reflectance was somehow nonlinear and reached its maximum for NiO_x of 100 nm thick and then decreased for thicker films, for which the absorbance was higher. Such results demonstrate that the film thickness is a critical parameter to consider if one aims at tuning the optical properties, especially the optical transparency in the vis region.

https://doi.org/10.1021/acsomega.3c05561
ACS Omega 2024, 9, 3295−3304

Table 3. List of Parameters Used in This Numerical Simulation Are Provided[56]

properties	*n*-Si	*p*-Si	*p*+-Si
thickness (μm)	5	20	20
band gap (eV)	1.12	1.12	1.12
electron affinity (eV)	4.05	4.05	4.05
dielectric permittivity	11.90	11.90	11.90
electron mobility [$cm^2/(V\ s)$]	1500	1500	1500
hole mobility [$cm^2/(V\ s)$]	450	450	450
electron and hole thermal velocity (cm/s)	1.65×10^7	1.65×10^7	1.65×10^7
acceptor conc. (cm^{-3})	1×10^1	1×10^{16}	5×10^{18}
donor conc. (cm^{-3})	1×10^{20}	1×10^1	1×10^1
effective conduction band density (cm^{-3})	2.80×10^{19}	2.80×10^{19}	2.80×10^{19}
effective valence band density (cm^{-3})	1.04×10^{19}	1.04×10^{19}	1.04×10^{19}
radiative recombination coefficient (cm^3/s)	2.3×10^{-9}	3×10^{-11}	3×10^{-11}

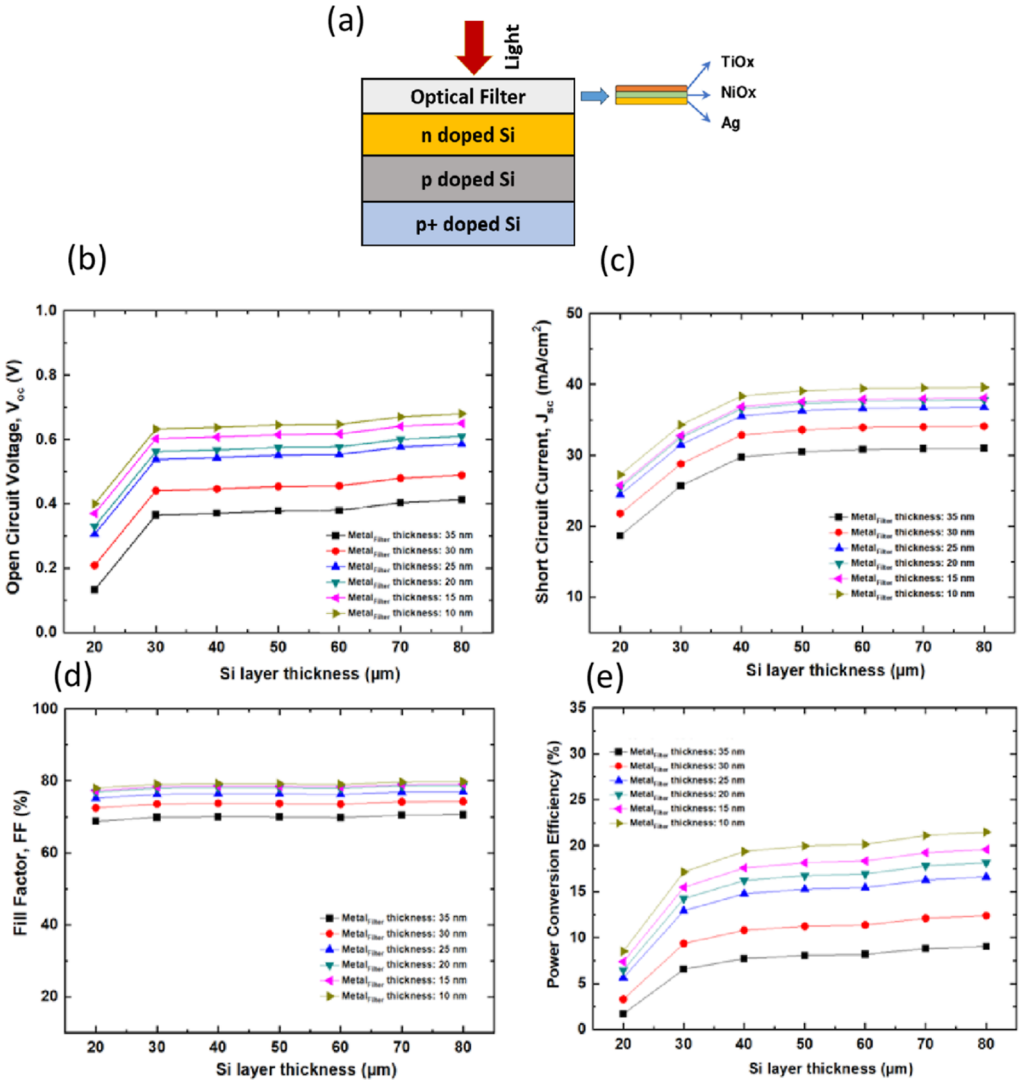

Figure 8. Device performance simulation of Si solar cells using the optical properties of NIR filters. (a) Schematic of the simulated device. (b) Open-circuit voltage (V_{oc}), (c) short-circuit current J_{sc} (mA/cm^2), (d) fill factor (FF %), and (e) power conversion efficiency (PCE %). The Ag metal layer thickness of the filter varied from 10 to 35 nm.

Figure 6a,b shows the *T* % and *R* % of 100 nm thick NiO_x deposited on 10 nm of Al and/or Ag layers. Figure 6c displays the variation of both *T* % and *R* % as a function of NiO film thicknesses, deposited on 10 nm thick Al and Ag, respectively. These optical properties show that Ag has a higher reflectance capacity in the IR than Al, where more than 50% of IR photons are reflected with a NiO_x film of 300 nm and a Ag metal mirror of only 10 nm.

Furthermore, TiO_x layers were grown on NiO/Ag/flexible polyethylene terephthalate (PET) substrates, as shown in Figure 7. PET was used for its high mechanical flexibility and to permit these filters to adapt and coat nonflat geometrical

https://doi.org/10.1021/acsomega.3c05561
ACS Omega 2024, 9, 3295−3304

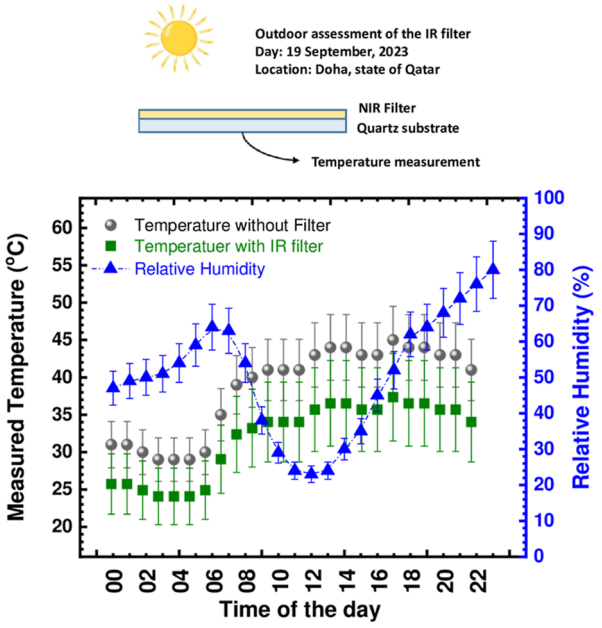

Figure 9. Temperature measurement vs time of the day performed on a quartz substrate placed in outdoor conditions, in cases with and without IR coating.

shapes. TiO_x, instead, is known for its self-cleaning property and has already been demonstrated as an antidust coating in desert environments.[58] Among all the tested configurations and the studied thicknesses, TiO_x (50 nm)/NiO (100 nm)/Ag (10 nm) and TiO_x (50 nm)/NiO (100 nm)/Ag (15 nm) have shown the highest IR reflection of more than 38% in the 750−1200 nm and an acceptable light transmittance of more than 50% in the visible region.[59−68]

Generally, the wetting behavior of thin layers with a specific contact angle can be used for antiadhesion and/or antisoiling applications.[47−52] However, this assumption is true only if it is correlated with the local weather environment. As a matter of fact, dry versus humid climates may recommend opposite wetting behavior, i.e., hydrophobic vs hydrophilic, and developing such antidust coatings must be subjected to assessment in a real-world environment before such a claim could be formulated. In our investigation, TiO_x (50 nm)/NiO (100 nm)/Ag (10 nm) showed maximum hydrophobicity with a contact angle of about 104°, whereas other stackings and thicknesses confirmed rather hydrophilic behavior. A previous study confirmed that surface wettability changes significantly with roughness.[53] An angle of 61.3° has been found for TiO_x (50 nm)/NiO (300 nm)/Ag (15 nm) due to the proportional roughness dependence.

3.4. Numerical Simulation. The numerical analysis was carried out using the following structure: TiO_x/NiO/Ag/*n*-Si/*p*-Si/p+-Si/metal contacts using the data shown in Table 3. The numerical analysis using SCAPS used the optical properties of the NIR filters as measured experimentally. The results are shown in Figure 8. The calculated values confirm that Si devices with the optimized optical filter [TiO_x (50 nm)/NiO (100 nm)/Ag (10 nm)] result in higher J_{sc} (39.60 mA/cm^2) and V_{oc} (680 mV). Short-circuit current (J_{sc}) increases significantly with the improvement of light-absorbing capacity within the Si absorber layer. A significant drop in PV performance occurs for metal thickness (Ag) ≥ 15 nm, which we attributed to the increasing reflection in the vis range occurring at the thicker metal layer in the filter.

The minimal achievable reflectance was calculated using OptiLayer software.[57] It includes the angle of incidence and s-polarization incidence along with an antireflection design having two points of refractive indices. In addition, OptiLayer software simulates the minimal reflectance for the dual-stage metal oxide layers including TiO_x and NiO_x layers for wavelengths ranging from 400 to 750 nm. The calculated results show that the fine-tuning of TiO_x/NiO can lead to a minimum reflectance of only 0.4%. Such results support the topic of developing an optimized ARC layer with an integrated IR filter to serve the double purposes of heat reduction and improving PV device performance.

Finally, we have demonstrated experimentally the capability of this IR filter with a reduction in cooling of up to 17.87% under outdoor conditions. The preliminary results are shown in Figure 9. However, it is essential to conduct a thorough assessment, reproducibility, and confirmation of these findings both outdoor and indoor, with an accurate quantification of the TR, and study the existing correlations of the TR with the dust deposition density, the relative humidity, and the wind speed over a longer period of time (one must target 12 months to cover the entire temperature range and the dusty and meteorological conditions over the year). Work is currently in progress.

4. SUMMARY

Photonic coolers based on IR filters are developed to cutoff wavelengths, which cause heat generation. In this work, stacked layers consisting of metal oxides and metal layers were developed by using a reactive e-beam evaporation process. The highest NIR cutoff was obtained for NiO (100 nm)/Ag (10 nm) layers with a value of 38% IR reflectance in the 750−1200 nm range while keeping a descent *T* % value above 50% in the vis range. Later, flexible substrates were used to develop such IR filters with other functionalities such as antireflection and antisoiling coatings. TiO_x (50 nm)/NiO (100 nm)/Ag (10 nm) showed the highest hydrophobicity, with a CA of about 104°. These results confirm that the developed multistacked metal-oxide/metal-oxide/metal layers using thermal e-beam evaporation can be used as a flexible NIR light filter with a potential antidust ability and a large-scale fabrication feasibility. The preliminary experimental results confirmed the capability of such filters to reduce the temperature in outdoor conditions efficiently. Work is currently in progress to quantify this reduction accurately and correlate it with dusty and meteorological conditions.

■ ASSOCIATED CONTENT

Data Availability Statement

The data that support the findings of this study are available from the corresponding author upon reasonable request.

■ AUTHOR INFORMATION

Corresponding Author

Brahim Aïssa − *Qatar Environment and Energy Research Institute (QEERI), Hamad Bin Khalifa University (HBKU), Doha, Qatar;* orcid.org/0000-0002-4768-9891; Email: baissa@hbku.edu.qa

https://doi.org/10.1021/acsomega.3c05561
ACS Omega 2024, 9, 3295−3304

Author

Mohammad Istiaque Hossain − *HBKU Core Laboratories, Hamad Bin Khalifa University (HBKU), Qatar Foundation, Doha, Qatar*

Complete contact information is available at: https://pubs.acs.org/10.1021/acsomega.3c05561

Notes

The authors declare no competing financial interest.

■ ACKNOWLEDGMENTS

The authors thank the HBKU Core Laboratories team for material characterizations.

■ REFERENCES

(1) Abundiz-Cisneros, N.; Sanginés, R.; Rodríguez-López, R.; Peralta-Arriola, M.; Cruz, J.; Machorro, R. Novel Low-E filter for architectural glass pane. *Energy Build.* **2020**, *206*, 109558.

(2) Zhao, P.; Kim, S.; Yoon, S.; Song, P. Characteristics of indium zinc oxide/silver/indium zinc oxide multilayer thin films prepared by magnetron sputtering as flexible transparent film heaters. *Thin Solid Layers* **2018**, *665*, 137−142.

(3) Loka, C.; Park, K. R.; Lee, K. S. Multi-functional TiO2/Si/Ag(Cr)/TiN coatings for low-emissivity and hydrophilic applications. *Appl. Surf. Sci.* **2016**, *363*, 439−444.

(4) Sahm, H.; Charton, C.; Thielsch, R. Oxidation behaviour of thin silver films deposited on plastic web characterized by spectroscopic ellipsometry (SE). *Thin Solid Layers* **2004**, *455*−*456*, 819−823.

(5) Hossain, M. I.; Khandakar, A.; Chowdhury, M. E. H.; Ahmed, S.; Nauman, M. M.; Aïssa, B. Numerical and Experimental Investigation of Infrared Optical Filter Based on Metal Oxide Thin Layers for Temperature Mitigation in Photovoltaics. *J. Electron. Mater.* **2021**, *51*, 1.

(6) Stamate, E. Spatially Resolved Optoelectronic Properties of Al-Doped Zinc Oxide Thin Films Deposited by Radio-Frequency Magnetron Plasma Sputtering Without Substrate Heating. *Nanomaterials* **2019**, *10*, 14.

(7) Tan, W. K.; Yokoi, A.; Kawamura, G.; Matsuda, A.; Muto, H. PMMA-ITO composite formation via electrostatic assembly method for infra-red filtering. *Nanomaterials* **2019**, *9*, 886.

(8) Liang, C.-H.; Chen, S.-C.; Qi, X.; Chen, C.-S.; Yang, C.-C. Influence of film thickness on the texture, morphology and electro-optical properties of indium tin oxide films. *Thin Solid Layers* **2010**, *519*, 345−350.

(9) Liang, C.-H.; Wang, W.-L.; Hwang, W.-S. High-rate and low-temperature growth of ZnO:Ga thin films by steered cathodic arc plasma evaporation. *Appl. Surf. Sci.* **2013**, *265*, 621−629.

(10) Liang, C.-H.; Chen, Y.-J. Preparation of High-Performance Metal-Free UV/Near Infrared-Shielding Films for Human Skin Protection. *Nanomaterials* **2021**, *11*, 1954.

(11) Choi, K. H.; Kim, J. Y.; Lee, Y. S.; Kim, H. J. ITO/Ag/ITO multilayer films for the application of a very low resistance transparent electrode. *Thin Solid Layers* **1999**, *341*, 152−155.

(12) Chu, C.-H.; Wu, H.-W.; Huang, J.-L. AZO/Au/AZO tri-layer thin films for the very low resistivity transparent electrode applications. *Mater. Sci. Eng., B* **2014**, *186*, 117−121.

(13) Kim, H.-K.; Lim, J.-W. Flexible IZO/Ag/IZO/Ag multilayer electrode grown on a polyethylene terephthalate substrate using roll-to-roll sputtering. *Nanoscale Res. Lett.* **2012**, *7*, 67.

(14) Kim, D.-H.; Cho, K.-S.; Kim, H.-K. Thermally evaporated indium-free, transparent, flexible SnO2/AgPdCu/SnO2 electrodes for flexible and transparent thin film heaters. *Sci. Rep.* **2017**, *7*, 2550.

(15) Zhao, S.; Ribbing, C.-G.; Wäckelgård, E. Optical constants of sputtered Ni/NiO solar absorber film—depth-profiled characterization. *Sol. Energy Mater. Sol. Cells* **2004**, *84*, 193−203.

(16) Majumder, S.; Bhattacharjee, S.; Ghosh, C. K. NiO/Ag heterostructure: enhanced UV emission intensity, exchange interaction, and photocatalytic activity. *RSC Adv.* **2016**, *6*, 56503−56510.

(17) Koçak, G.; Bütün, V.; Tuncer, C. Production of NiO, NiO/Ag, NiO/Au, and NiO/Pt hollow spheres by using block copolymer stabilized microspheres as a template. *Mater. Sci. Eng., B* **2021**, *138*, 51299.

(18) Valouch, S.; Robert, S. E. N. D.; Bruder, I.; Hermes, W. Infrared optical detector with integrated filter. WO 2018077870 A1, 2018.

(19) Teich, A. C.; Terre, W. A.; Boulanger, P.; Frank, J. D.; Distelzweig, J. H. Hybrid infrared sensor array having heterogeneous infrared sensors. U.S. Patent 10,110,833 B2, 2018.

(20) Alanson, D. A.. Semiconductor device and manufacture thereof. U.S. Patent 3,763,404 A, 1972.

(21) Leem, D. S.; Kim, K. S.; Kim, J. W.; Park, K. B.; Lee, K. H.; Lim, S. J. Light transmissive electrode, organic photoelectric device, and image sensor. U.S. Patent 9,379,343 B2, 2016.

(22) Hermes, W.; Valouch, S.; Send, R.; Bruder, I.; Feuerstein, B. Database rollback using wal. U.S. Patent 20,160,321,143 A1, 2019.

(23) Jiang, J.; Love, R. T.; Yang, S. Apparatus with Vis and infrared light-emitting display. U.S. Patent 10,151,946 B2, 2018.

(24) Powell, K. D.; Dighde, R. M. Sensor-in-pixel display system with near infrared filter. U.S. Patent 8,749,529 B2, 2014.

(25) Wang, J. T.-W.; Ball, J. M.; Barea, E. M.; Abate, A.; Alexander-Webber, J. A.; Huang, J.; Saliba, M.; Mora-Sero, I.; Bisquert, J.; Snaith, H. J.; et al. Low-temperature processed electron collection layers of graphene/TiO2 nanocomposites in thin film perovskite solar cells. *Nano Lett.* **2014**, *14*, 724−730.

(26) Pinpithak, P.; Chen, H.-W.; Kulkarni, A.; Sanehira, Y.; Ikegami, M.; Miyasaka, T. Low-temperature and Ambient Air Processes of Amorphous SnOx-based Mixed Halide Perovskite Planar Solar Cell. *Chem. Lett.* **2017**, *46*, 382−384.

(27) Liu, C.; Li, W.; Chen, J.; Fan, J.; Mai, Y.; Schropp, R. E. Ultra-thin MoOx as cathode buffer layer for the improvement of all-inorganic CsPbIBr2 perovskite solar cells. *Nano Energy* **2017**, *41*, 75−83.

(28) Cao, K.; Zuo, Z.; Cui, J.; Shen, Y.; Moehl, T.; Zakeeruddin, S. M.; Grätzel, M.; Wang, M. Efficient screen printed perovskite solar cells based on mesoscopic TiO2/Al2O3/NiO/carbon architecture. *Nano Energy* **2015**, *17*, 171−179.

(29) Mazur, M.; Wojcieszak, D.; Domaradzki, J.; Kaczmarek, D.; Song, S.; Placido, F. TiO2/SiO2 multilayer as an antireflective and protective coating deposited by microwave-assisted magnetron sputtering. *Opto-Electron. Rev.* **2013**, *21*, 233−238.

(30) Green, M. A.; Ho-Baillie, A.; Snaith, H. J. The emergence of perovskite solar cells. *Nat. Photonics* **2014**, *8*, 506−514.

(31) Kumar, L. S.; Bhatt, D.; Karthikeyan, S. Influence of Hole and Electron Transport Materials on Perovskite Sensitized Solar Cells-A Review. *J. Environ. Nanotechnol.* **2016**, *5*, 48−64.

(32) Ye, M.; He, C.; Iocozzia, J.; Liu, X.; Cui, X.; Meng, X.; Rager, M.; Hong, X.; Liu, X.; Lin, Z. Recent advances in interfacial engineering of perovskite solar cells. *J. Phys. D: Appl. Phys.* **2017**, *50*, 373002.

(33) Baroch, P.; Musil, J.; Vlcek, J.; Nam, K.; Han, J. Reactive magnetron sputtering of TiO films. *Surf. Coat. Technol.* **2005**, *193*, 107−111.

(34) Leja, E.; Korecki, J.; Krop, K.; Toll, K. Phase composition of SnOx thin films obtained by reactive d.c. sputtering. *Thin Solid Layers* **1979**, *59*, 147−155.

(35) Fernandes Cauduro, A. L.; Fabrim, Z. E.; Ahmadpour, M.; Fichtner, P. F.; Hassing, S.; Rubahn, H.-G.; Madsen, M. Tuning the optoelectronic properties of amorphous MoOx films by reactive sputtering. *Appl. Phys. Lett.* **2015**, *106*, 202101.

(36) Velevska, J.; Ristova, M. Electrochromic properties of NiOx prepared by low vacuum evaporation. *Sol. Energy Mater. Sol. Cells* **2002**, *73*, 131−139.

(37) Bullock, J.; Cuevas, A.; Allen, T.; Battaglia, C. Molybdenum oxide MoOx: A versatile hole contact for silicon solar cells. *Appl. Phys. Lett.* **2014**, *105*, 232109.
(38) Yao, J.; Shao, J.; He, H.; Fan, Z. Optical and electrical properties of TiOx thin films deposited by electron beam evaporation. *Vacuum* **2007**, *81*, 1023−1028.
(39) Yang, X.; Zheng, P.; Bi, Q.; Weber, K. Silicon heterojunction solar cells with electron-selective TiOx contact. *Sol. Energy Mater. Sol. Cells* **2016**, *150*, 32−38.
(40) Whang, S.-J.; Lee, S.; Chi, D.-Z.; Yang, W.-F.; Cho, B.-J.; Liew, Y. F.; Kwong, D.-L. B-doping of vapour-liquid-solid grown Au-catalyzed and Al-catalyzed Si nanowires: effects of B2H6 gas during Si nanowire growth and B-doping by a post-synthesis in situ plasma. *Nanotechnology* **2007**, *18*, 275302.
(41) Macco, B.; Vos, M.; Thissen, N.; Bol, A.; Kessels, W. Low-temperature atomic layer deposition of MoOx for silicon hetero-junction solar cells. *Phys. Status Solidi RRL* **2015**, *9*, 393−396.
(42) Kim, I. S.; Jeong, E.-K.; Kim, D. Y.; Kumar, M.; Choi, S.-Y. Investigation of p-type behavior in Ag-doped ZnO thin films by E-beam evaporation. *Appl. Surf. Sci.* **2009**, *255*, 4011−4014.
(43) Hossain, M. I.; Zakaria, Y.; Zikri, A.; Samara, A.; Aissa, B.; El-Mellouhi, F.; Hasan, N. S.; Belaidi, A.; Mahmood, A.; Mansour, S. A. E-beam evaporated hydrophobic metal oxide thin films as carrier transport materials for large scale perovskite solar cells. *Materials Technology* **2022**, *37*, 248−259.
(44) Payne, B. P.; Biesinger, M. C.; McIntyre, N. S. X-ray photoelectron spectroscopy studies of reactions on chromium metal and chromium oxide surfaces. *J. Electron Spectrosc. Relat. Phenom.* **2011**, *184*, 29−37.
(45) Rashid, H.; Rahman, K. S.; Hossain, M. I.; Nasser, A. A.; Alharbi, F. H.; Akhtaruzzaman, M.; Amin, N. Physical and electrical properties of molybdenum thin films grown by DC magnetron sputtering for photovoltaic application. *Results Phys.* **2019**, *14*, 102515.
(46) Ponchel, A.; D'Huysser, A.; Lamonier, C.; Jalowiecki-Duhamel, L. CeNixOy and CeAlzNixOy solids studied by electron microscopy, XRD, XPS and depth sputtering techniques. *Phys. Chem. Chem. Phys.* **2000**, *2*, 303−312.
(47) Lafuma, A.; Quéré, D. Superhydrophobic states. *Nature materials.* **2003**, *2*, 457−460.
(48) Fürstner, R.; Barthlott, W.; Neinhuis, C.; Walzel, P. Wetting and self-cleaning properties of artificial superhydrophobic surfaces. *Langmuir* **2005**, *21*, 956−961.
(49) Blossey, R. Self-cleaning surfaces—virtual realities. *Nature materials.* **2003**, *2*, 301−306.
(50) Miwa, M.; Nakajima, A.; Fujishima, A.; Hashimoto, K.; Watanabe, T. Effects of the surface roughness on sliding angles of water droplets on superhydrophobic surfaces. *Langmuir* **2000**, *16*, 5754−5760.
(51) Cheng, Y. T.; Rodak, D. E. Is the lotus leaf superhydrophobic? *Appl. Phys. Lett.* **2005**, *86*, 144101.
(52) Feng, X. J.; Jiang, L. Design and creation of superwetting/antiwetting surfaces. *Adv. Mater.* **2006**, *18*, 3063−3078.
(53) Hossain, M. I.; Aïssa, B.; Samara, A.; Mansour, S. A.; Broussillou, C. A.; Benito, V. B. Hydrophilic antireflection and antidust silica coatings. *ACS Omega* **2021**, *6*, 5276−5286.
(54) Bal, S. S.; Basak, A.; Singh, U. P. Numerical modeling and performance analysis of Sb-based tandem solar cell structure using SCAPS-1D. *Opt. Mater.* **2022**, *127*, 112282.
(55) Belarbi, M.; Zeggai, O.; Louhibi-Fasla, S. Numerical study of Methylammonium Lead Iodide Perovskite solar cells using SCAPS-1D simulation program. *Mater. Today: Proc.* **2022**, *51*, 2115−2119.
(56) Shawky, T. A.; Aly, M. H.; Fedawy, M. Performance analysis and simulation of c-Si/SiGe based solar cell. *IEEE Access* **2021**, *9*, 75283−75292.
(57) OptiLayer. 2020. https://www.optilayer.com/images/Booklet_OptiLayer.pdf (accessed 4 June 2023).
(58) Fares, E.; Aïssa, B.; Isaifan, R. Inkjet printing of metal oxide coatings for enhanced photovoltaic soiling environmental applications. *Global J. Environ. Sci. Manage.* **2022**, *8*, 485.
(59) Shen, L. S.; Wu, H. Y.; Hsiao, L. J.; Shih, C. H.; Hsu, J. C. LED Light Improved by an Optical Filter to Visible Solar-Like Light with High Color Rendering. *Coatings* **2021**, *11*, 763.
(60) Ma, X.; Zhai, Y.; Ji, J.; Wu, Z.; Wang, Q. The optical properties of a visible light filter integrated on the silicon substrate. *Opt. Commun.* **2020**, *464*, 125510.
(61) Zakirullin, R. Creating optical filters with angular-selective light transmission. *Appl. Opt.* **2015**, *54*, 6416−6419.
(62) Sticklus, J.; Hieronymi, M.; Hoeher, P. A. Effects and constraints of optical filtering on ambient light suppression in LED-based underwater communications. *Sensors* **2018**, *18*, 3710.
(63) Badgujar, A. C.; Yadav, B. S.; Jha, G. K.; Dhage, S. R. Room temperature sputtered aluminum-doped ZnO thin film transparent electrode for application in solar cells and for low-band-gap optoelectronic devices. *ACS Omega* **2022**, *7*, 14203−14210.
(64) https://chromogenics.com/dynamic-glass/ (accessed 5 June 2023).
(65) Lee, M.; Kim, G.; Jung, Y.; Pyun, K. R.; Lee, J.; Kim, B. W.; Ko, S. H. Photonic structures in radiative cooling. *Light: Sci. Appl.* **2023**, *12*, 134.
(66) Iqbal, M.; Nauman, M. M.; Khan, F. U.; Abas, P. E.; Cheok, Q.; Iqbal, A.; Aissa, B. Multimodal hybrid piezoelectric-electromagnetic insole energy harvester using PVDF generators. *Electronics* **2020**, *9*, 635−636.
(67) Farahani, R. D.; Dalir, H.; Le Borgne, V.; Gautier, L. A.; El Khakani, M. A.; Lévesque, M.; Therriault, D. Reinforcing epoxy nanocomposites with functionalized carbon nanotubes via biotin-streptavidin interactions. *Compos. Sci. Technol.* **2012**, *72*, 1387−1395.
(68) Aïssa, B.; El Khakani, M. A. The channel length effect on the electrical performance of suspended-single-wall-carbon-nanotube-based field effect transistors. *Nanotechnology* **2009**, *20*, 175203.

https://doi.org/10.1021/acsomega.3c05561
ACS Omega 2024, 9, 3295−3304